

Chaotic transport in reversed shear tokamaks

F.A. Marcus¹, T. Kroetz², M. Roberto², I.L. Caldas¹,
E.C. da Silva¹, R.L. Viana^{3,a} and Z.O. Guimarães-Filho¹

¹ Instituto de Física, Universidade de São Paulo, 05315-970, São Paulo, São Paulo, Brazil

² Instituto Tecnológico de Aeronáutica, Centro Técnico Aeroespacial, Departamento de Física, 12228-900, São José dos Campos, São Paulo, Brazil

³ Departamento de Física, Universidade Federal do Paraná, 81531-990, Curitiba, Paraná, Brazil

E-mail: viana@fisica.ufpr.br

Received 11 May 2007, accepted for publication 6 September 2007

Published 30 January 2008

Online at stacks.iop.org/NF/48/024018

Abstract

For tokamak models using simplified geometries and reversed shear plasma profiles, we have numerically investigated how the onset of Lagrangian chaos at the plasma edge may affect the plasma confinement in two distinct but closely related problems. Firstly, we have considered the motion of particles in drift waves in the presence of an equilibrium radial electric field with shear. We have shown that the radial particle transport caused by this motion is selective in phase space, being determined by the resonant drift waves and depending on the parameters of both the resonant waves and the electric field profile. Moreover, we have shown that an additional transport barrier may be created at the plasma edge by increasing the electric field. In the second place, we have studied escape patterns and magnetic footprints of chaotic magnetic field lines in the region near a tokamak wall, when there are resonant modes due to the action of an ergodic magnetic limiter. A non-monotonic safety factor profile has been used in the analysis of field line topology in a region of negative magnetic shear. We have observed that, if internal modes are perturbed, the distributions of field line connection lengths and magnetic footprints exhibit spatially localized escape channels. For typical physical parameters of a fusion plasma, the two Lagrangian chaotic processes considered in this work can be effective in usual conditions so as to influence plasma confinement. The reversed shear effects discussed in this work may also contribute to evaluate the transport barrier relevance in advanced confinement scenarios in future tokamak experiments.

PACS numbers: 52.55.Fa, 52.55.Lf, 52.35.Mw, 52.55.Dy, 52.25.Gj

1. Introduction

Many experiments carried out in the last decade have confirmed long-standing claims that plasma confinement in toroidal devices strongly depends on the electric and magnetic fields at the plasma edge [1–5]. The former fields are related to the observed anomalous particle transport at the plasma edge, which has been shown to be largely controlled by low-frequency electrostatic drift waves [2]. The steep density and temperature gradients existing in the plasma edge give rise to diamagnetic currents across the confining toroidal magnetic field so generating drift waves propagating in the poloidal direction. Drift instabilities occur along this process, such that particle thermal energy is converted in wave energy, the corresponding fields causing the chaotic motion of plasma particles typically related to anomalous diffusion.

^a Author to whom any correspondence should be addressed.

As for the magnetic fields, chaotic field lines at the plasma edge have been found to play a key role in plasma-wall interactions in tokamaks [6–8]. One of the possible effects of chaotic field lines is the concentration of heat and particle loadings on the tokamak wall, which deteriorates the overall plasma confinement quality [9–11]. Chaotic field line transport, however, is to be taken in the Lagrangian sense, meaning spatial separation of nearby field lines *at fixed time*, when the magnetic field line configuration is non-integrable [12–14].

Since charged plasma particles follow magnetic field lines to leading order, it appears natural to think of anomalous diffusion arising from some combination of the above mentioned electric and magnetic fields. On the other hand, things are not so simple for even uniform magnetic fields may cause chaotic particle gyration when suitable electrostatic waves are applied [15]. Hence a comprehensive description of anomalous particle diffusion would have to take into account

the possible existence of *both* electric and magnetic fields at plasma edge. The complexity of the energy transfer among waves and particles makes it difficult to directly attack this problem by, e.g. computer codes based on a kinetic description of particles interacting with electric and magnetic fields chaotic in space and time. In spite of such difficulties, some common issues exist such that we can grasp some physically interesting issues from the isolated analysis of chaotic magnetic and electric fields.

One of the common features of complex electric and magnetic field structures in the tokamak plasma edge is the existence of reversed shear, which has been given a great deal of attention in recent years, since they arise in advanced tokamak scenarios [16]. Electric and magnetic reversed shear fields are considered separately in this work with respect to their influences on the transport of particles and field lines, respectively, in the plasma edge region.

Reversed magnetic shear in tokamaks is possible when the plasma current radial profiles are non-monotonic such that the field line rotational transform possesses a simple maximum or minimum for some radius, which we call *shearless radius* from now on. As a consequence, the field line map is non-twist, i.e. it does not satisfy the so-called twist condition. Since the field line map is two-dimensional and area-preserving (for a divergenceless magnetic field), the twist condition can be expressed in the following form: points more radially displaced from the wall make larger jumps in the poloidal direction [17]. The field line map we obtained for reversed-field configurations fail to satisfy this condition due to the existence of a shearless radius.

Reversed shear also occurs for the radial electric field related to drift waves, in the plasma edge region, and causes a $\mathbf{E} \times \mathbf{B}$ force which drives particles into a reversed shear drift flow with a wide variety of experimentally observed effects. We performed numerical simulations of particle motion by solving the canonical equations from a drift-kinetic Hamiltonian considering the action of two waves with a phase-difference, leading to a non-integrable system, for which there are periodic, quasi-periodic and chaotic trajectories.

Our main goal in this paper is to investigate possible effects from electric and magnetic reversed shear fields on plasma confinement through a combination of numerical simulation results and concepts from Hamiltonian theory. Whereas the electric reversed shear is tractable from direct integration of particle equations of motion, the magnetic reversed shear requires the obtention of a field line map. We kept the models for both electric and magnetic reversed shear fields as simple as possible so as to isolate their effects on the particle and field line transport. Accordingly, for the electric reversed shear field the magnetic field is monotonic and vice versa. However, many interesting phenomena stem from considering simultaneously both forms of shear, like the possible obtention of a high-confinement mode for tokamak discharges [18–20]. For the magnetic reversed shear equilibrium field we have added the field of an ergodic magnetic limiter so as to generate non-integrable field line configurations and Lagrangian chaos. Our numerical simulations used parameters taken from the Brazilian tokamak TCABR, for which an ergodic limiter has been designed to control plasma oscillations [21]. As far as other tokamaks are concerned, ergodic limiters have been used

to improve plasma confinement in TORE SUPRA [22–24], TEXTOR [25] and DIII-D [26].

The rest of this paper is organized as follows: in section 2 we consider the electric reversed shear configuration through the interaction of particles with one and two electrostatic waves in a monotonic magnetic field. Section 3 deals with the magnetic reversed shear case by presenting the model fields for the tokamak non-monotonic equilibrium field and the ergodic limiter perturbation. We show the obtention of a field line map, and our numerical results concerning escape patterns and magnetic footprints. Our conclusions are left to the last section.

2. Drift wave transport in reversed shear flows

Experiments indicate that the plasma edge behaviour depends on the anomalous particle transport caused by the observed electrostatic turbulence [2]. Thus, it is important to estimate the contribution to this transport due to chaotic particle orbits driven by the turbulent fluctuation. To do that, in this work we study the transport of particles in a magnetically confined plasma due to electrostatic drift waves. The adopted model describes the trajectory of the guiding centre of a particle in a uniform magnetic field perpendicular to a radial electric field perturbed by drift waves [27].

We have used the Hamiltonian description for the guiding centre trajectory. The $\mathbf{E} \times \mathbf{B}$ drift produced by the equilibrium radial electric field and a dominant wave is represented by the integrable part of the Hamiltonian, while the other part contains the perturbation representing the fluctuating electric field associated to other drift waves. We study the resonances and island chains created at the plasma edge and associate the anomalous plasma edge transport to the Lagrangian chaotic transport of the guiding centres of ions [27]. In this way we obtain chaotic orbits that determine the particle radial transport [28, 29]. We have used the experimental data of electrostatic turbulence measured in TCABR tokamak to obtain realistic predictions.

Single particle motion in one drift wave is described by an integrable Hamiltonian system and can be solved analytically. For a resonant wave, a two-dimensional lattice of counter rotating rolls separated by a separatrix is created in the resonant region. The particles cannot cross the separatrix so that they are confined to motion within a single roll [27]. The second wave, with an amplitude smaller than that of the first wave, is treated as a perturbation. The Hamiltonian is no longer time-independent such that a particle is no longer confined to a single roll [27]. Thus, qualitative features of this transport can be approximated by a low-dimensional dynamical system with island chains in phase space due to the superposition of two dominant drift waves. For experimental parameters usually observed in tokamaks, we analyse the onset of chaos in this system.

We describe the superposition of poloidal drift waves as a Hamiltonian system without dissipation. The drift velocity of the guiding centres are given by [27]

$$\vec{v} = \frac{\vec{E} \times \vec{B}}{B^2}, \quad \vec{E} = -\nabla\phi, \quad (1)$$

which is equivalent, in the slab approximation and using polar cylindrical coordinates, to the following set of differential equations:

$$v_r = \frac{dr}{dt} = -\frac{1}{rB_0} \frac{\partial}{\partial \theta} \phi(r, \theta), \quad (2)$$

$$v_\theta = \frac{d\theta}{dt} = \frac{1}{B_0} \frac{\partial}{\partial r} \phi(r, \theta), \quad (3)$$

representing canonical equations obtained from the Hamiltonian as

$$H(r, \theta, t) = \frac{\phi(r, \theta, t)}{r_0 B_0}, \quad (4)$$

for a uniform magnetic field.

We describe the electrical potential $\phi(r, \theta, t)$ at the plasma edge as the superposition of an equilibrium term $\phi_0(r)$ and N electrostatic drift waves

$$\phi(r, \theta, t) = \phi_0(r) + \sum_{i=1}^N C_i \sin(k_{r_i} r) \cos(k_{\theta_i} \theta - \omega_i t). \quad (5)$$

Substituting (5) into equation (4) and dividing by E_0/B_0 yields a dimensionless Hamiltonian given by

$$H(r, \theta, t) = H_0(r) + \sum_{i=1}^N A_i \sin(k_{r_i} r) \cos(k_{\theta_i} \theta - \omega_i t). \quad (6)$$

Moreover, in order to investigate the effects of reversed electric field we choose a potential with a non-monotonic radial profile

$$\phi_0(r) = ar^3 + br^2 + cr, \quad (7)$$

where a , b , and c are dimensionless parameters whose values can be fit to the background potential measured at the tokamak edge.

In this work we consider the cases of both one ($N = 1$) and two drift waves ($N = 2$), which represents an integrable and a non-integrable Hamiltonian system, respectively, the latter typically presenting chaotic behaviour depending on the perturbation strength and the initial conditions chosen. We can remove the time dependence in the first wave by performing a canonical transformation

$$r = r' \quad \text{and} \quad \theta' = \theta - \frac{\omega_1}{k_{\theta_1}} t, \quad (8)$$

such that the transformed Hamiltonian reads (omitting the primes in the variables for notational simplicity),

$$H(r, \theta, t) = ar^3 + br^2 + (c - u_1)r + A_1 \sin(k_{r_1} r) \cos(k_{\theta_1} \theta) + A_2 \sin(k_{r_2} r) \cos[k_{\theta_2}(\theta - ut)], \quad (9)$$

where $u = u_2 - u_1 \equiv (\omega_2/k_{\theta_2}) - (\omega_1/k_{\theta_1})$ is the phase difference between the waves. This transformation corresponds to a change to a frame moving with the phase velocity u_1 of the first wave.

Let us begin by the integrable case of only one wave ($A_2 = 0$), for which the Hamiltonian is given by

$$H(r, \theta) = ar^3 + br^2 + (c - u_1)r + A_1 \sin(k_{r_1} r) \cos(k_{\theta_1} \theta). \quad (10)$$

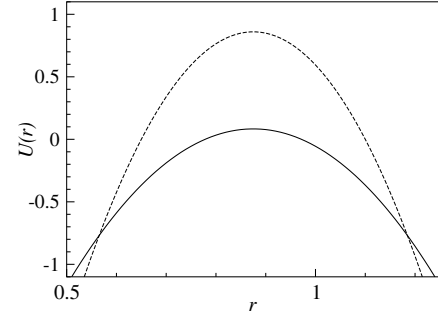


Figure 1. Radial profiles A (full curve) and B (dashed curve) of the trapping parameter $U(r)$ for the case of a non-monotonic electric field.

The corresponding canonical equations have a single relevant dimensionless parameter, the trapping parameter given by

$$U(r) = \frac{3ar^2 + 2br + (c - u_1)}{A_1 k_{r_1}} = \frac{-E_r - u_1}{A_1 k_{r_1}}, \quad (11)$$

which describes the influence of the wave parameters and the normalized electric field on the radial transport of the guiding centres. The resonant condition, $u_1 = -E_r$, occurs at those radii \bar{r} given by $U(\bar{r}) = 0$. Figure 1 presents the two radial profiles of the trapping parameter, which we call A and B hereafter, which correspond to radial electric field profiles and phase velocities of two kinds of discharges observed in the Brazilian tokamak TCABR. This is a ohmically-heated tokamak with hydrogen circular plasma, with major radius $R = 61$ cm and minor radius $a = 18$ cm. The plasma current reaches a maximum value of 100 kA, with duration 100 ms, the hydrogen filling pressure is 3×10^{-4} Pa and toroidal magnetic field $B_T = 1.1$ T [30].

Figure 2(a) depicts a phase space plot for the integrable Hamiltonian system consisting of the profile A and one wave ($A_2/A_1 = 0$). Without the second wave there is no chaos and the phase space exhibits some periodic structures where $U \approx 0$, consisting of islands chains centred at fixed points. The particular island chain, occurring at the radial location wherein $U(\bar{r}) = 0$, turns to be the place where the second wave will act more intensively generating a chaotic layer. Such a resonant island chain occurs at $\bar{r} \approx 0.87$, which is also the location of the elliptic (o-) points at the centres of those islands. The poloidal positions of these points are $\bar{\theta}_j = \pi j/12$, for $j = 0, 1, 2, \dots, 24$. The widths of the islands belonging to this chain can be estimated from the positions of the hyperbolic (x-) points adjacent to this specific chain, and which are located at $\bar{r}_1 \approx 0.94$ and $\bar{r}_2 \approx 0.80$, their poloidal positions being $\bar{\theta}_j = (\pi/12)(j + 1/2)$, with $j = 0, 1, 2, \dots, 24$.

On the other hand, for $|U| \approx 1$, we see barriers acting to limit the particle radial transport so effectively helping in the confinement of the particle guiding centres. This occurs in two different regions, one is the scrape-off layer next to the tokamak inner wall, and the second is the internal part of the plasma edge. In fact, tokamak experiments have pointed out that the quality of plasma confinement may increase with the rise of the radial electric field when the tokamak wall is polarized by a bias voltage [30]. In addition, we have observed that this may be also produced by the electric field of drift waves of

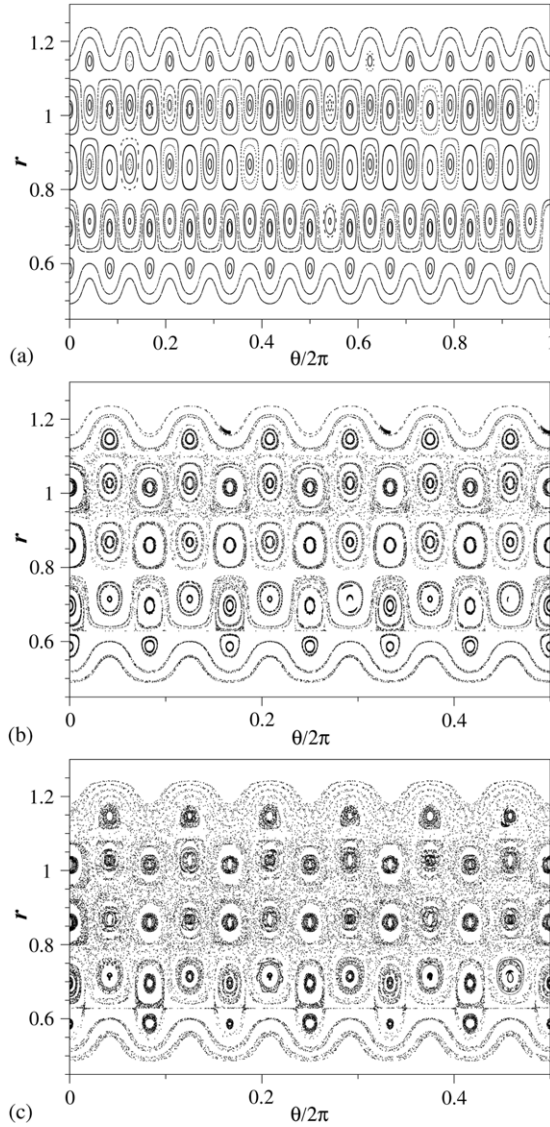


Figure 2. Phase space plots for the drift Hamiltonian (9) with the non-monotonic profile A and (a) $A_2/A_1 = 0$; (b) $A_2/A_1 = 0.1$ and (c) $A_2/A_1 = 0.4$. Note the island chains created at the shearless radius $\bar{r} \approx 0.87$.

suitable phase velocity and wave amplitude, according to the behaviour of the trapping parameter U .

The superposition of two drift waves turns the Hamiltonian system into a non-integrable one, with the consequent breakdown of a number of invariant curves (in the phase plane) and the consequent formation of homoclinic chaos. Figure 2(b) shows the perturbed phase plot (for a shorter poloidal angle interval for the sake of a better visualization) obtained by adding a second wave with amplitude $A_2 = 0.1A_1$ to the integrable system of one wave. The separatrix orbits connecting the hyperbolic points are the first ones to become chaotic when the second wave is added. The orbits near the elliptic points remain closed, while orbits near the hyperbolic points are chaotic, filling some nonzero area in the phase plane with a bounded radial excursion, thus contributing to particle diffusion along this direction. Increasing the amplitude of the second wave to $A_2 = 0.4A_1$ (figure 2(c)), we observe chiefly the enlargement of the chaotic layer. Small islands of stability

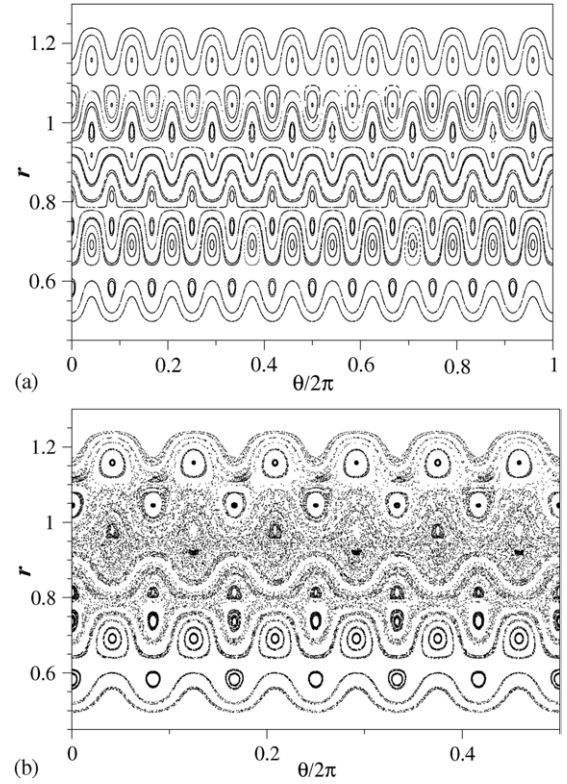


Figure 3. Phase space plot for the drift Hamiltonian (9) with the non-monotonic profile B and (a) $A_2/A_1 = 0$; (b) $A_2/A_1 = 0.4$. An additional barrier appears with an average radial coordinate $\langle \bar{r} \rangle \approx 0.85$.

still exist near the elliptic points, but large scale diffusion takes place due to the more pronounced radial excursion of orbits throughout the chaotic layer.

In figures 3(a) and (b) we consider the non-monotonic equilibrium profile B for one and two waves, respectively. The overall characteristics are kept unchanged here, but we see that an additional barrier appears in the region for which $U \approx 1$ separating the island chains seen in the previous figures. This barrier appears due to the electric field increase according to the profile B. As a consequence of this variation, the orbit stochasticization is reduced to the internal part of the plasma edge. This result shows that the transport can be reduced by increasing the radial electric field.

3. Connections lengths and magnetic footprints with reversed magnetic shear

A second problem related to reversed field and transport is the influence of a reversed magnetic shear on the field line structure in a tokamak already perturbed such that there is a region of Lagrangian chaos for magnetic field lines. The field line map so derived has been used in previous works to investigate the homoclinic tangles underlying chaotic field line regions in the outer tokamak region, when monotonic safety profiles are used [31, 32]. The formation of a transport barrier, in the case of non-monotonic profiles, has been also put into evidence with help of this map [33]. In this paper we consider such a non-monotonic profile from the point of view of magnetic footprints and connection lengths.

The field line geometry can be described by using the non-orthogonal polar-toroidal coordinates $(r_t, \theta_t, \varphi_t)$, given by [34]

$$r_t = \frac{R'_0}{\cosh \xi - \cos \omega}, \quad \theta_t = \pi - \omega, \quad \varphi_t = \Phi, \quad (12)$$

where R'_0 is the magnetic axis radius and (ξ, ω, Φ) are the toroidal coordinates. The coordinate surfaces $r_t = \text{constant}$ are displaced with respect to the tokamak minor axis so as to emulate the Shafranov shift effect [34]. Magnetic surfaces are characterized by nested surfaces of $r_t = \text{constant}$, for which the safety factor is [33]

$$q_c(r_t) = q_c(a) \frac{r_t^2}{a^2} \left[1 - \left(1 + \beta' \frac{r_t^2}{a^2} \right) \left(1 - \frac{r_t^2}{a^2} \right)^{\gamma+1} \Theta \left(1 - \frac{r_t}{a} \right) \right]^{-1}, \quad (13)$$

with

$$q_c(a) \equiv \frac{I_p a^2}{I_e R_0'^2}, \quad (14)$$

where I_p is the total plasma current, a is the plasma radius, I_e is the external current that generates the equilibrium toroidal field, and the parameters γ and β , with

$$\beta' \equiv \beta \frac{(\gamma + 1)}{(\beta + \gamma + 2)} \quad (15)$$

describing the plasma current profile [33,35]. In the following, we will choose $q \approx 5$ at the plasma edge ($r_t = a$). For a non-monotonic safety factor profile, there is a region of negative magnetic shear as well as a shearless radius. We adopt $\gamma = 0.80$ and $\beta = 3.00$ so as to have $q \approx 4.80$ at the magnetic axis. We will also choose parameters so that $a/R'_0 = 0.26$, which is a typical value for tokamaks [36].

Since the equilibrium magnetic field is axisymmetric, we may set the ignorable coordinate φ_t as a time-like variable, t (to be used as a field line parametrization), and put the field line equations in a Hamiltonian form [17]. This enables us to define angle-action variables (\mathcal{J}, ϑ) for an equilibrium Hamiltonian given by

$$H_0(\mathcal{J}) = 2\pi \int \frac{d\mathcal{J}}{q(r_t(\mathcal{J}))}. \quad (16)$$

The explicit form of the relations between these angle-action variables and the toroidal polar coordinates can be found in [37]. The equilibrium flux surfaces exhibit the Shafranov shift with respect to the geometrical minor axis and thus are not concentric with the tokamak wall, which is at a fixed position $\mathcal{J} = 0.055$ determined by the radius of the material limiter. Figure 4 shows a non-monotonic safety factor profile for a tokamak equilibrium field for which the safety factor at the plasma edge is $q(a) = 5$. The concavity of the profile is so as to have a shearless radius near $\mathcal{J} = 0.02$. We see that there are two radii for which the safety factor is equal to 4.0, for instance. As a consequence, a perturbation resonant with this mode will create two island chains centred at these radii.

We consider an ergodic magnetic limiter design which consists of N_r slices of a pair of resonant helical windings, with adequate mode numbers and equally positioned along the toroidal direction (see [37]). The design of the helical windings needs to take into account the effects of the toroidal geometry, which makes the toroidal magnetic field component stronger in the inner side of the torus than in the outer one.

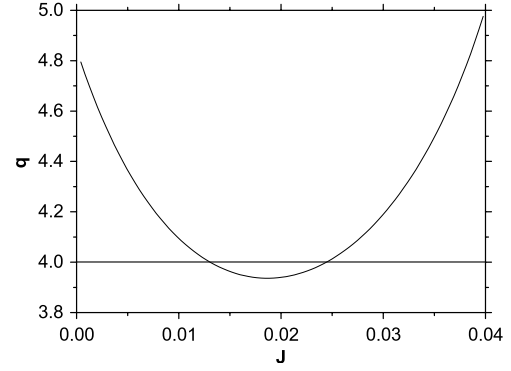


Figure 4. Non-monotonic safety factor profile in terms of the action variable \mathcal{J} and corresponding to an equilibrium field with $\gamma = 0.80$, $\beta = 2.00$ and $q(a) = 5$.

Consequently, the magnetic field line pitch is nonuniform. We use a winding law that emulates the actual paths followed by magnetic field lines. A tunable parameter, λ , is introduced such that the variable $u_t = m_0[\theta_t + \lambda \sin(\theta_t)] - n_0\varphi_t$, where (m_0, n_0) are the poloidal and toroidal mode numbers, respectively, is constant along a field line.

A perturbing Hamiltonian, $H_1(\mathcal{J}, \vartheta, t)$, describing the action of the EMLs, is obtained from the magnetic field generated by the helical windings. This magnetic field is an approximated analytical solution of the Laplace equation, supposing a vacuum field (valid for low-beta plasma only) [37]. The boundary conditions are written down with help of a singular current distribution located at the tokamak wall. Although the equilibrium Hamiltonian $H_0(\mathcal{J})$ is integrable, the addition of a non-symmetric perturbation, $H_1(\mathcal{J}, \vartheta, t)$, caused by the EML rings, breaks the integrability of the system. Therefore, we model the action of the EML rings on the equilibrium magnetic field lines as a sequence of pulses described by the following one-and-a-half degree of freedom Hamiltonian:

$$H(\mathcal{J}, \vartheta, t) = H_0(\mathcal{J}) + \epsilon H_1(\mathcal{J}, \vartheta, t) \sum_{k=-\infty}^{\infty} \delta \left(t - k \frac{2\pi}{N_r} \right). \quad (17)$$

Due to the t -dependence of the Hamiltonian in the form of a sequence of delta-functions, it is possible to define discretized variables $(\mathcal{J}_n, \vartheta_n)$ as the corresponding values of the angle-action variables just after the n -th crossing of a field line with the plane $t_k = (2\pi k/N_r)$ with $k = 0, 1, 2, \dots, N_r - 1$. The area-preserving mapping obtained from the Hamiltonian (17) can be found in [37]. Figure 5(a) shows a Poincaré cross-section produced by our area-preserving mapping, where we choose $\gamma = 0.80$ and $\beta = 3.00$ corresponding to the non-monotonic q profile of figure 4. The perturbing parameter $\lambda = 0.45319$ is used in order to focus the perturbation on the most external surface with $q = 4$. The chaotic region closer to the tokamak wall which is seen in figure 5(a) comes from a usual resonance overlapping scenario. Due to the integrability breakdown not just the resonant magnetic surfaces, but every rational surface (namely those with rational values for their safety factors) yields an island chain. The distinctive feature of resonant perturbations is that they produce larger islands than they do in non-resonant magnetic surfaces. As the safety factor

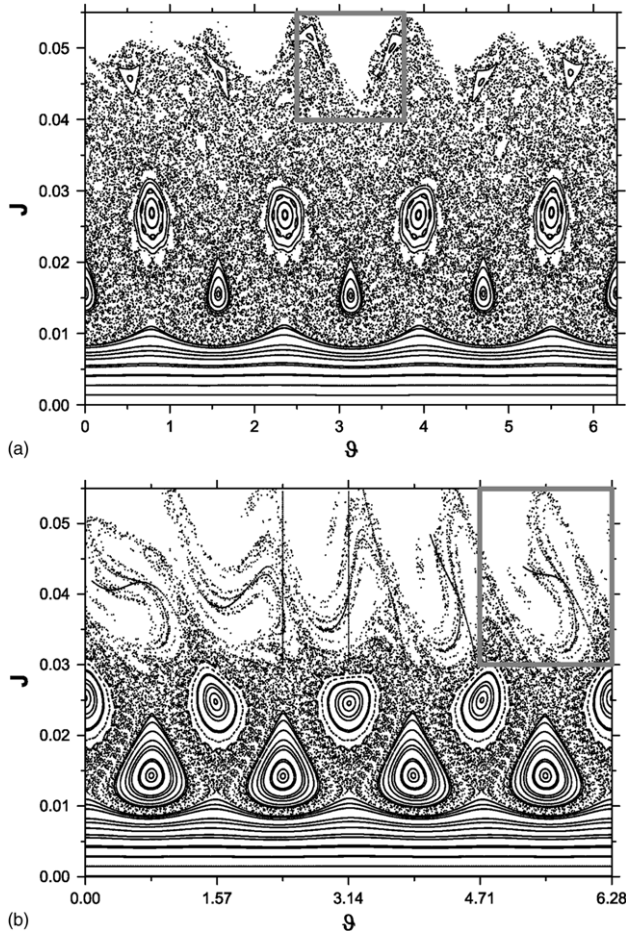


Figure 5. Example of the Poincaré cross-section produced by the EML mapping, in terms of the action-angle variables (J, ϑ), for a non-monotonic q profile with $\gamma = 0.80$ and $\beta = 3.000$, $N_r = 4$, $\lambda = 0.45319$, $I_h = 8.5\%$ of I_p and (a) $(m_0, n_0) = (4, 1)$, (b) $(m_0, n_0) = (5, 1)$.

near the tokamak wall is monotonic (without shear reversals), KAM theory holds again permitting the creation of chaotic regions at the tokamak edge.

Next, we analyse the connection lengths and the magnetic footprints of the chaotic region obtained for a non-monotonic safety profile, in order to investigate the effect of using non-twist mappings on the escape patterns on the tokamak wall. The cases of resonances closer and farther from the wall are considered. In order to obtain the connection lengths we use a grid of 500×500 points chosen inside the small rectangle shown in figure 5(a), and which comprises a representative part of the chaotic region near the wall. We iterate each point of the grid until the line reach the wall ($\mathcal{J} = 0.055$). The connection lengths N_{CL} indicate how many turns are necessary for the toroidal field line to strike the tokamak wall, and can take on values in a wide interval, from $N_{CL} = 1$ to $N_{CL} \approx 10^4$.

In order to examine field lines with small connection lengths we consider those values of N_{CL} covering an interval from 1 to 10, to which different shades of gray are assigned. Accordingly, black pixels correspond to field lines which do not escape until 4000 iterations have been elapsed, and can be considered as trapped. Figure 6(a) shows the connection lengths for this case. One can observe that the initial conditions

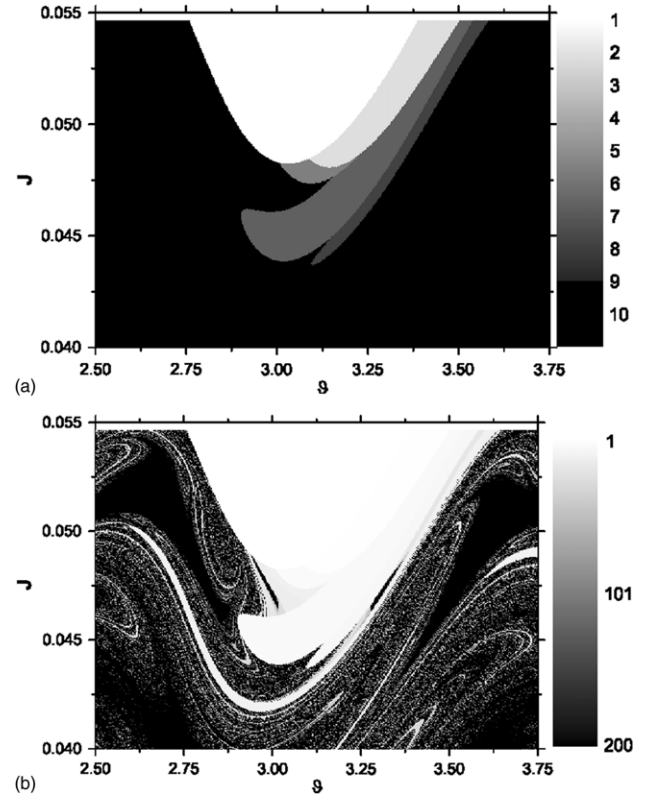


Figure 6. (a) Connection lengths for the EML map shown in figure 5(a). The lengths of the field lines belong to the interval $[1, 10]$ and are represented in gray-scale. (b) The lengths of the field lines are in the range $[1, 200]$.

with $N_{CL} > 10$ saturate in a fixed shade of gray. Figure 6(b) shows the connection length for $N_{CL} = 1-200$. They have a fractal pattern. These results were obtained for a limiter with mode numbers $(4, 1)$, which intercepts the tokamak wall at preferential regions. We can alter the limiter parameters so as to generate a chaotic region which touches the wall in more and wider intervals. Figure 5(b) shows this possibility and presents a Poincaré mapping with the grid of initial conditions for mode numbers $(5, 1)$ and the same perturbation current as in the former case. Figures 7(a) and (b) show the connection lengths for both small and large values of N_{CL} . We observed that initial conditions generating orbits with low N_{CL} correspond to regions with smooth boundaries in the phase portraits, whereas initial conditions related to large values of N_{CL} form regions with a fractal boundary structure.

Neglecting the thickness of the vessel wall, we can set the tokamak wall at the same radius as the ergodic limiter rings themselves $r_t = r_w$. Suppose that a chaotic region does intercept this constraint at one or more intervals. It is thus necessary to impose that a field line is considered lost once it reaches this radial position. The magnetic footprints are the deposition patterns of field lines from the chaotic region and which are lost due to collisions with this constraint [38]. The escape time N_{ET} is the number of iterations it takes for a given field line to hit this point. We observed that the escape time is related with the density of points in the Poincaré plots, in the sense that those field lines belonging to densely populated regions take more time to escape (hitting the tokamak wall) than those field lines in sparsely populated regions.

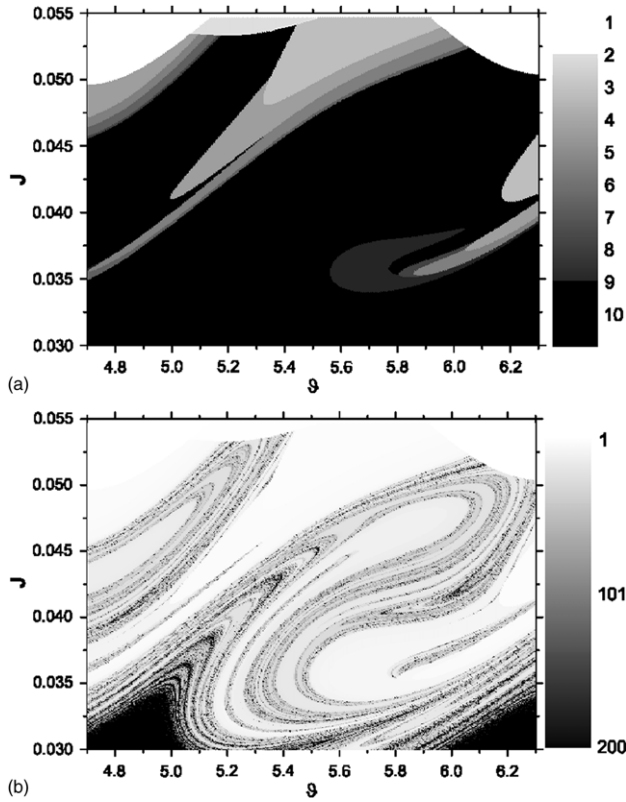


Figure 7. (a) Connection lengths for the EML map shown in figure 5(b). The lengths of the field lines belong to the interval [1, 10] and are represented in grey-scale. (b) The lengths of the field lines are in the range [1, 200].

Field lines tend to escape following the unstable manifolds of periodic orbits embedded in the chaotic region, i.e. such manifolds, which have an involved fractal structure, form channels of preferential escape [31, 39, 40]. For this reason, the magnetic footprints resulting from collisions of field lines with the tokamak wall present likewise a fractal structure. For the non-monotonic profile used in this work, the magnetic footprints are shown in figures 8(a) and (b), where we can see the dependence of the escape time N_{ET} with the poloidal angle ϑ_f , for initial conditions chosen uniformly along the poloidal cross section. For many intervals there is no field line incidence. On the other hand, there are abrupt variations in some intervals, revealing very involved, and actually fractal structures.

Figure 8(a) was obtained for a limiter with mode numbers $(m_0, n_0) = (4, 1)$, for which the chaotic region intercepts the tokamak wall in two narrow intervals. Altering the limiter parameters generates a chaotic region which touches the wall in other intervals. Figure 8(b) demonstrates this possibility for mode numbers $(m_0, n_0) = (5, 1)$. Instead of two centred escape channels, we now have at least five channels. These fractal regions with high N_{ET} values not always correspond to regions with many field lines. The resonance excited by mode numbers (4, 1) turned out to be deeper (i.e. farther from the wall) than the resonance induced by (5, 1). Hence, when comparing the chaotic regions for both cases, with a nearly equal limiter current, we expect the chaotic region of the latter intercepting more points of the wall than the former. This is

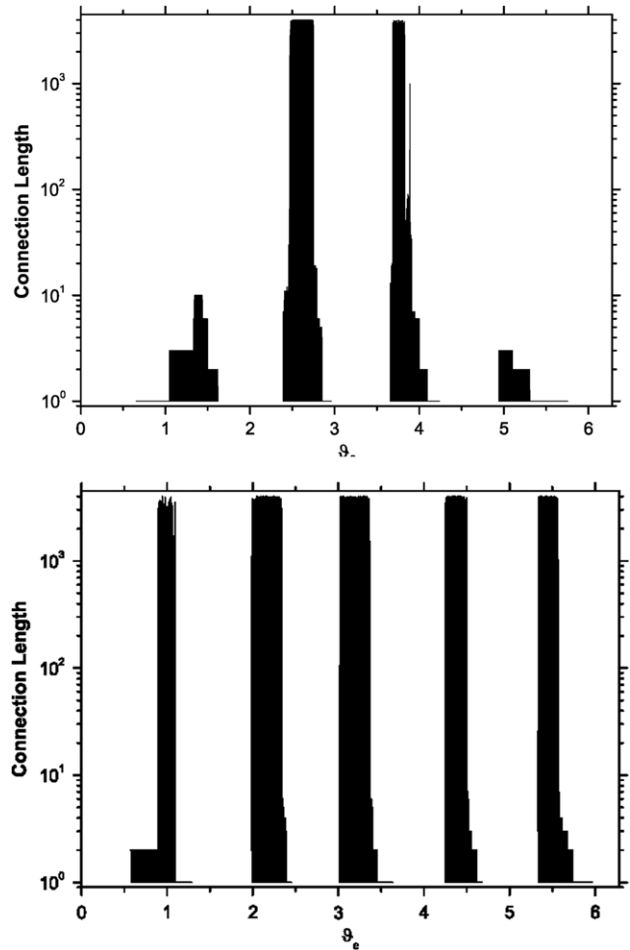


Figure 8. (a) The magnetic footprints for the parameters of figure 5(a). (b) The parameters are those of figure 5(b).

not really unexpected, since the radial location of the (4, 1) resonance is slightly less than of the (5, 1) one. Even though we are dealing here with a non-monotonic safety profile, the interval to which both resonances belong has a positive magnetic shear, i.e. it is an effectively monotonic increasing profile for that region.

4. Conclusions

In this work we applied the Lagrangian chaos theory, considering fusion plasma parameters for simplified tokamak geometries. We discussed two effects observed at the plasma edge, namely, the chaotic anomalous particle transport from the $\mathbf{E} \times \mathbf{B}$ drift motion, as well as the distribution of chaotic magnetic field lines at the wall.

Initially, we explored a dynamical mechanism by which the particle transport is achieved and showed how alterations on the electric field radial profile at the plasma edge can modify this transport within this region. Thus, guiding centre trajectories can be stochastized by this process within the region where the trapping parameter vanishes. On the other hand, by increasing the trapping parameter a particle transport barrier can appear at this region.

After that, we showed that the number and the distribution of the escape channels are determined by two factors: the mean

width of the chaotic region and the resonance from which it starts. The former depends in a complicated fashion on the limiter current, whereas the second is dictated by the shape of the safety current profile in the region of interest. Our results suggest that the deeper is the resonance from which the chaotic region starts, the more concentrated are the deposition patterns due to the existence of less escape channels.

In the design of experiments of the sort described in this paper, we propose that, if the limiter current cannot be raised above some levels, it would be better to use resonances near the wall, provided there are non-monotonic profiles. However, we must remark that our conclusions were drawn from a rather simplified model and thus more comparisons should be performed with experiments conducted in machines like DIII-D [7, 26] and TEXTOR [1, 6] tokamaks on controlled plasma edge transport.

Acknowledgments

This work was made possible through partial financial support from the following Brazilian government agencies: FAPESP (São Paulo), CNPq, CAPES, and Fundação Araucária (Paraná).

References

- [1] Abdullaev S.S., Finken K.H., Jakubowski M.W., Kasilov S.V., Kobayashi M., Reiser D., Reiter D., Runov A.V. and Wolf R. 2003 *Nucl. Fusion* **43** 299
- [2] Horton W. 1999 *Rev. Mod. Phys.* **71** 735
- [3] Balescu R. 2005 *Aspects of Anomalous Transport in Plasmas* (London: Taylor and Francis)
- [4] Alejaldre C. *et al* 1999 *Plasma Phys. Control. Fusion* **41** B109
- [5] Hidalgo C. *et al* 2005 *Nucl. Fusion* **45** S266
- [6] Jakubowski M.W. *et al* 2006 *Phys. Rev. Lett.* **96** 35004
- [7] Evans T.E. *et al* 2005 *J. Nucl. Mater.* **337** 691
- [8] McCool S.C. *et al* 1989 *Nucl. Fusion* **29** 547
- [9] Post D.E. and Behrisch R. 1986 *Physics of Plasma–Wall Interactions in Controlled Fusion* (New York: Plenum)
- [10] Parker R., Janeschitz G., Pacher H.D., Post D.E., Chiocchio S., Federici G. and Ladd P. 1997 *J. Nucl. Mater.* **241–243** 1
- [11] Stangeby P.C. 2000 *The Plasma Boundary of Magnetic Fusion Devices* (Bristol: Institute of Physics Publishing)
- [12] Meiss J.D. 1992 *Rev. Mod. Phys.* **64** 795
- [13] Morrison P.J. 1998 *Rev. Mod. Phys.* **70** 467
- [14] Boozer A.H. 2004 *Rev. Mod. Phys.* **76** 1071
- [15] Smith G.R. and Pereira N.R. 1978 *Phys. Fluids* **21** 2253
- [16] Mazzucato E. *et al* 1996 *Phys. Rev. Lett.* **77** 3145
- [17] Morrison P.J. 2000 *Phys. Plasmas* **7** 2279
- [18] Kwon J.-M., Horton W., Zhu P., Morrison P.J., Park H.-B. and Choi D.I. 2000 *Phys. Plasmas* **7** 1169
- [19] Weysow B., Misguich J.H. and Balescu R. 1991 *Plasma Phys. Control. Fusion* **33** 763
- [20] El Monden M., Saifaoui D., Dezaini A., Zine B. and Eddahby M. 2007 *J. Plasma Phys.* **73** 439
- [21] Heller M.V.A.P., Caldas I.L., Ferreira A.A., Saettone E.A.O., Vannucci A. and Nascimento I.C. 2005 *Czech. J. Phys.* **55** 265
- [22] Evans T.E., Goniche M., Grosman A., Guilhem D., Hess W. and Vallet J.C. 1992 *J. Nucl. Mater.* **196–198** 421
- [23] Boedo J.A. *et al* 2005 *Phys. Plasmas* **12** 72516
- [24] Moyer R.A. *et al* 2005 *Phys. Plasmas* **12** 56119
- [25] Jakubowski M.W., Abdullaev S.S., Finken K.H. and the TEXTOR Team 2004 *Nucl. Fusion* **44** S1
- [26] Evans T.E., Roeder R.K.W., Carter J.A. and Rapoport B.I. 2004 *Contrib. Plasma Phys.* **44** 235
- [27] Horton W. 1985 *Plasma Phys. Control. Fusion* **27** 937
- [28] Osipenkov I. 2000 Diffusion in chaotic systems *MSc Dissertation, Report IFSR #885* Institute for Fusion Studies, The University of Texas at Austin
- [29] Marcus F.A. Dynamic instability of tokamak electrostatic fluctuations *MSc Dissertation* IFUSP, São Paulo, unpublished (in portuguese)
- [30] Nascimento I.C. *et al* 2005 *Nucl. Fusion* **45** 796
- [31] da Silva E.C., Caldas I.L., Viana R.L. and Sanjuán M.A.F. 2002 *Phys. Plasmas* **9** 4917
- [32] Portela J.S.E., Caldas I.L., Viana R.L. and Morison P.J. 2007 *Int. J. Bifurcat. Chaos* **17** 1589
- [33] Roberto M., da Silva E.C., Caldas I.L. and Viana R.L. 2004 *Phys. Plasmas* **11** 214
- [34] Kucinski M.Y., Caldas I.L., Monteiro L.H.A. and Okano V. 1990 *J. Plasma Phys.* **44** 303
- [35] Oda G.A. and Caldas I.L. 1995 *Chaos Solitons Fractals* **5** 15
- [36] Corso G., Oda G.A. and Caldas I.L. 1997 *Chaos Solitons Fractals* **8** 1891
- [37] Caldas I.L., Viana R.L., Vannucci A., da Silva E.C., Araujo M.S.T., Ullmann K., Heller M.V.A.P. and Kucinski M.Y. 2002 *Braz. J. Phys.* **32** 980
- [38] da Silva E.C., Caldas I.L. and Viana R.L. 2001 *IEEE Trans. Plasma Sci.* **29** 617
- [39] Abdullaev S.S., Finken K.H., Kaleck A. and Spatschek K.H. 1998 *Phys. Plasmas* **5** 196
- [40] Abdullaev S.S., Finken K.H. and Spatschek K.H. 1999 *Phys. Plasmas* **6** 153
- [41] Abdullaev S.S., Th. Eich and Finken K.H. 2001 *Phys. Plasmas* **8** 2739
- [42] Grebogi C., Ott E. and Yorke J.A. 1983 *Physica D* **7** 181
- [43] Silva E.C., Roberto M., Caldas I.L. and Viana R.L. 2006 *Phys. Plasmas* **13** 52511